APPENDIX A
ADDITIONAL EXPERIMENTS

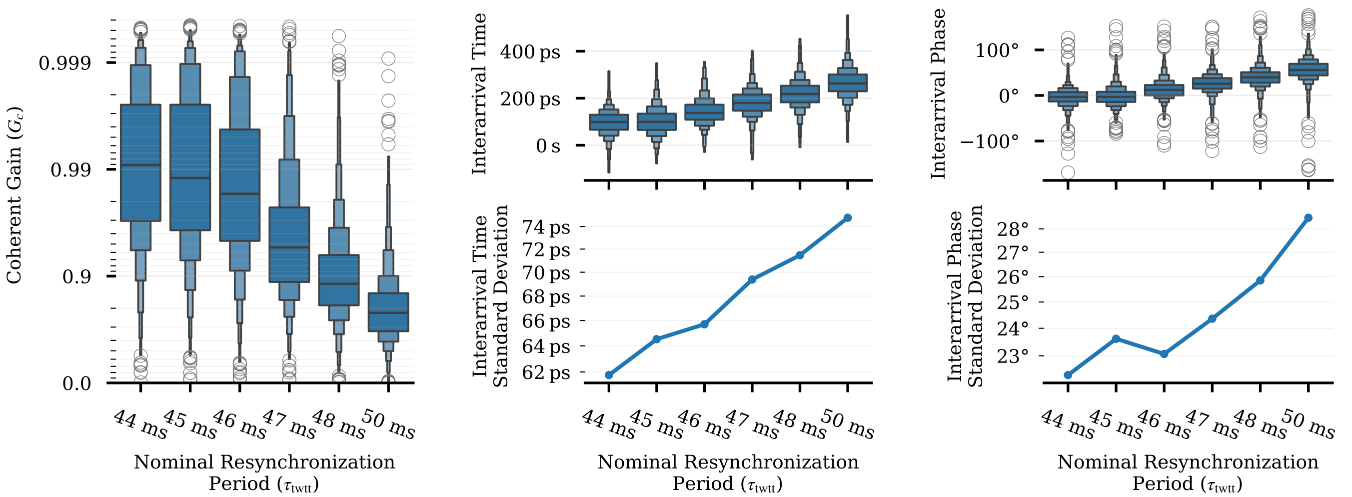

Fig. A.1. Electrical state coordination performance evaluation under varying resynchronization periods τ_{twtt}. The top row shows the absolute measured quantity; the bottom row shows the standard deviation. In the interarrival time standard deviation, the outliers have been removed as discussed in Section V-C. Across all measurements, an average Pre-integration SNR of approximately $\mu = 24\,\mathrm{dB}$ and $\sigma = 1$ was estimated.

1) Resynchronization Period: This experiment used *Configuration A* to evaluate coordination performance under varying resynchronization period τ_{twtt}, shown in Fig. A.1. The nominal resynchronization period was varied from 44 ms—the minimum possible on the host due to software implementation and hardware limitations—to 50 ms, at which the coherent gain performance begins to significantly decline due to the dominant system dynamics evolving faster than the resynchronization period.

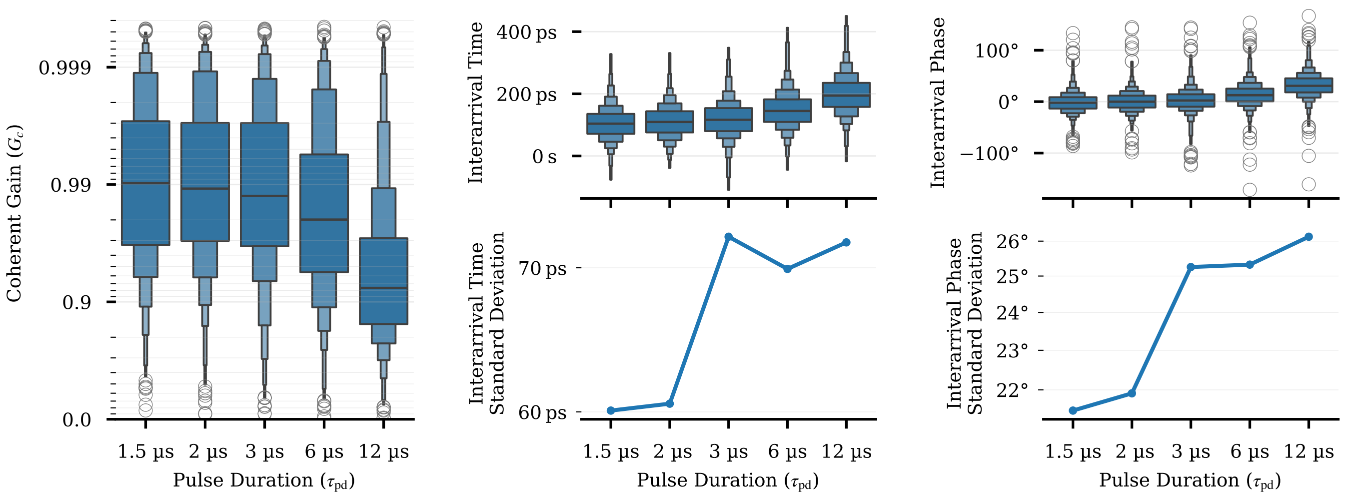

Fig. A.2. Electrical state coordination performance evaluation under varying TWTT PTT durations τ_{pd}. The top row shows the absolute measured quantity, and the bottom row shows its standard deviation, omitting outliers as discussed in Section V-C. Across all measurements, an average pre-integration SNR of approximately $\mu = 24\,\mathrm{dB}$ and $\sigma = 1$ was estimated for 1.5 µs–3.0 µs; however, due to an error, the SNR estimator did not correctly estimate 1.5 µs–3.0 µs, but similar SNRs are expected due to an identical system setup.

2) Two-Way Time Transfer Pulse Duration: This experiment used *Configuration A* to evaluate coordination performance under varying TWTT PTT durations τ_{pd}, shown in Fig. A.2. In these experiments the interpulse spacing is held constant while τ_{pd} is varied. According to (22), this should improve the time of arrival estimation; however, in practice, this increases the number of samples in the received pulse since the entire synchronization epoch is captured in a single receive frame on each software-defined radio (SDR), which increases the number of samples required to process, increasing the computation latency, yielding decreasing performance as shown in Fig. A.3. The long tail at $\tau_{\mathrm{pd}} = 12\,\mu\mathrm{s}$ is due to increased frequency of failure to meet real-time requirements due to the increased computational load of the matched filter. The interarrival delay and phase trends associated with the resynchronization period align with the varying resynchronization periods shown in Fig. A.1,

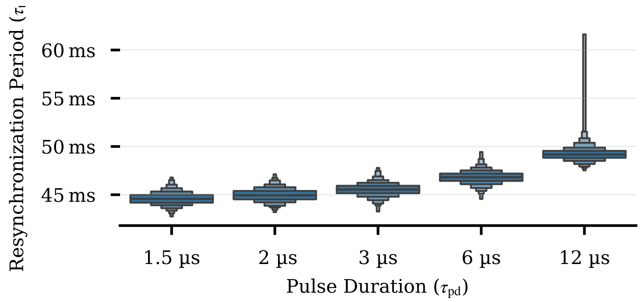

Fig. A.3. Resynchronization periods observed for various pulse durations. Results can be compared with those of Fig. A.1 to determine expected performance due to resynchronization period at each pulse duration.

suggesting the degradation is due mostly to the processing latency increase—not the pulse duration itself—which is expected as the electrical states are not expected to be significantly varying over single or tens of microseconds.

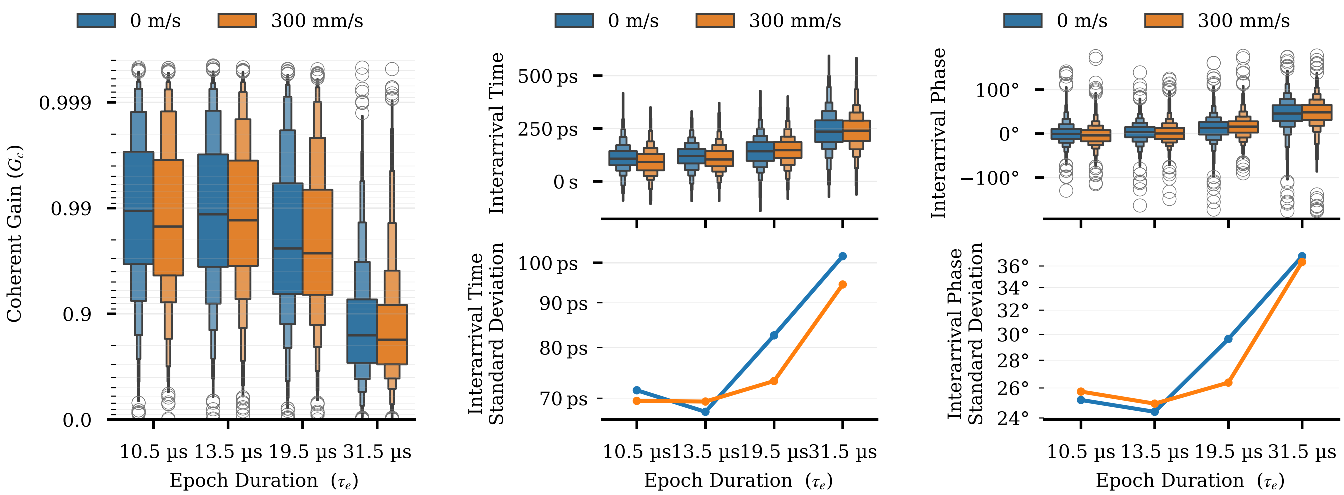

Fig. A.4. Electrical state coordination performance evaluation under varying TWTT synchronization epoch durations τ_e under static and dynamic relative motion. The top row shows the absolute measured quantity, and the bottom row shows its standard deviation, omitting outliers as discussed in Section V-C. In the static measurements, an average pre-integration SNR of approximately $\mu = 24\,\mathrm{dB}$ and $\sigma = 1$ was estimated; in the dynamic measurements the average pre-integration SNRs were approximately $\mu = 25.4\,\mathrm{dB}$ and $\sigma = 1.5$.

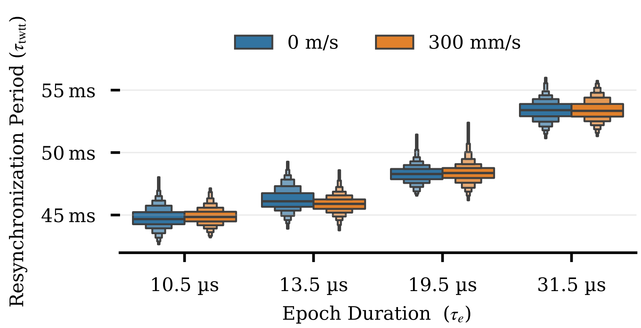

Fig. A.5. Resynchronization periods observed for various synchronization epoch durations under static and dynamic relative motion. Results can be compared with those of Fig. A.1 to determine expected performance due to resynchronization period at each epoch duration.

3) Synchronization Epoch Duration: This experiment used *Configuration A* to evaluate coordination performance over varying TWTT synchronization epoch durations τ_e for both a static system and a system with relative internode motion, shown in Fig. A.4. In these experiments, the antenna on node 0 was varied between 0 mm/s and 300 mm/s while the synchronization epoch duration was increased from 10.5 µs to 31.5 µs. Similarly to the pulse duration experiments, due to the increased number of samples to process as the synchronization epoch duration increases, the latency increases, shown in Fig. A.5; these again align with the performance degradations expected from the resynchronization shown in Fig. A.1 and show little correlation with static versus moving platforms, again suggesting these degradations are due primarily to the increased latency due to the increased number of samples required to be processed via the matched filter per synchronization epoch.

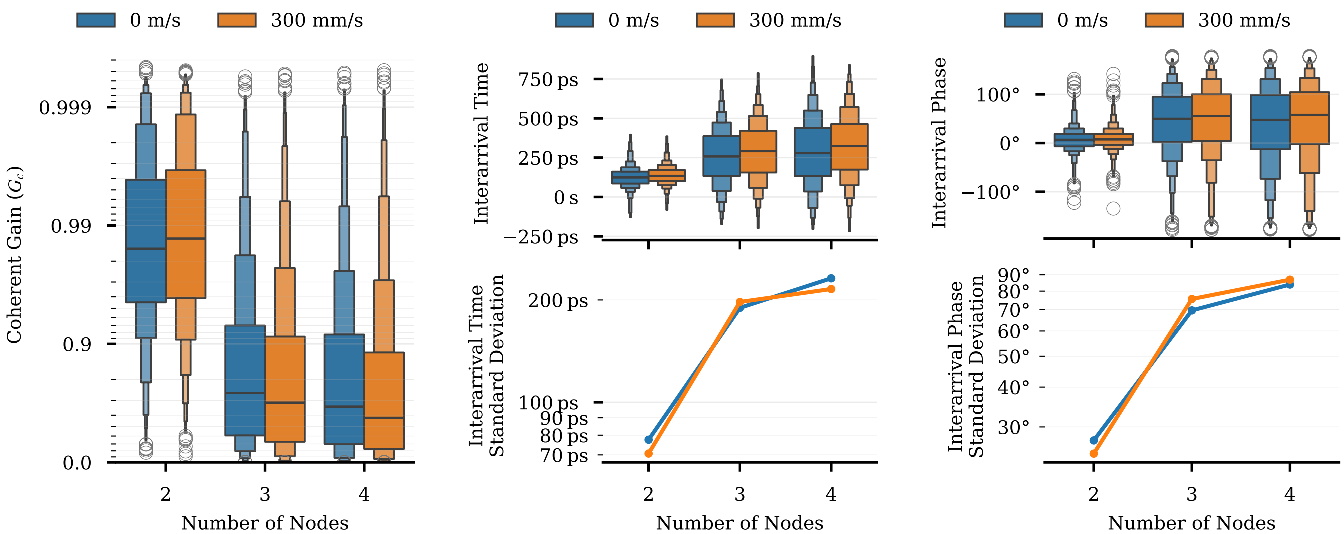

Fig. A.6. Electrical state coordination performance evaluation for various array sizes under static and dynamic relative motion. The top row shows the absolute measured quantity, and the bottom row shows its standard deviation, omitting outliers as discussed in Section V-C. Across all measurements, an average pre-integration SNR of approximately $\mu = 24\,\text{dB}$ and $\sigma = 1$ was estimated for two and three nodes; in the four-node array, the average pre-integration SNRs were approximately $\mu = 27\,\text{dB}$ and $\sigma = 1$.

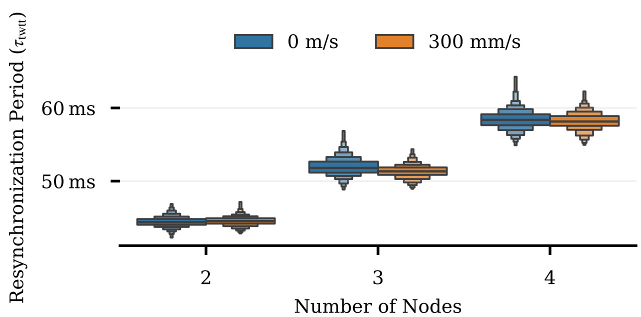

Fig. A.7. Resynchronization periods observed for various array sizes. Results can be compared with those of Fig. A.1 to determine expected performance due to resynchronization period at each array size.

4) Node Scaling: This experiment used *Configuration A* to evaluate the coordination performance for arrays of 2 to 4 nodes, shown in Fig. A.6. Beamforming data was only collected from nodes N_0 and N_1; however, as nodes were added, their time division multiple access (TDMA) slots were scheduled in between nodes N_0 and N_1 to illustrate the worst-case performance due to the longest synchronization epoch. As the number of nodes increases, the number of TDMA time slots in the TWTT also scales linearly, thus increasing the number of samples required to perform matched filtering on to compute the time of arrival (ToA) estimates for the TWTT process, increasing latency and decreasing synchronization performance, as discussed previously. The resynchronization interval statistics for this experiment are summarized in Fig. A.7. It is worth noting that even though the TWTT could be conducted using space, frequency, or code orthogonality, instead of time orthogonality, the number of samples required to be matched filtered is constant in all cases.

APPENDIX B
SUPPLEMENTAL FIGURES AND TABLES

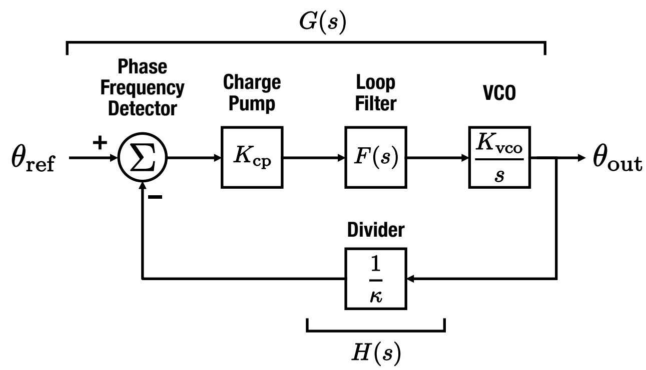

Fig. B.1. Simplified PLL synthesizer model. Noise is added at each stage in the loop and the frequency and noise are magnified by the feedback ratio κ.

TABLE B-I
SYNCHRONIZATION REFINEMENT PARAMETERS

Sync. Index (sync_idx)	Sample Rate ($f_{\mathrm{s,adc}}$; $f_{\mathrm{s,dac}}$)	Tone Separation (β_{ptt})	TDMA Window Duration (τ_{tdma})
0	10 MSa/s	1 MHz	10 ms
1	10 MSa/s	1 MHz	1.11 ms
2	200 MSa/s	20 MHz	122.47 µs
3	200 MSa/s	20 MHz	13.55 µs
4	200 MSa/s	20 MHz	1.5 µs

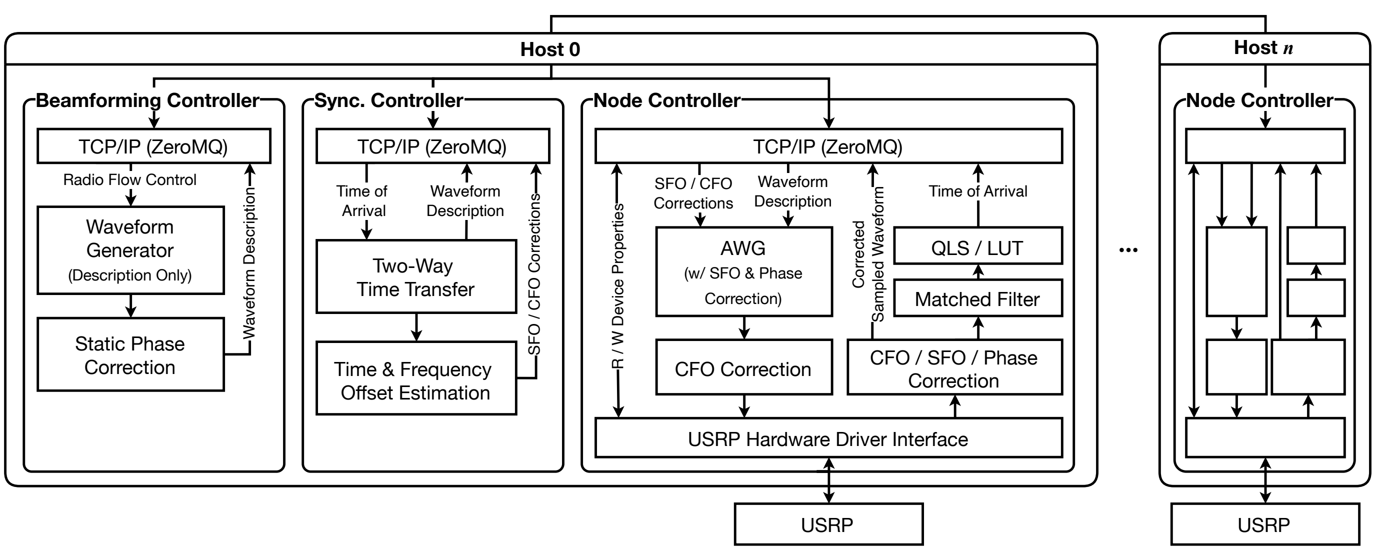

Fig. B.2. Software flow graph. Software utilized a centralized topology where Host 0 is running the Synchronization Controller and Beamforming Controller to orchestrate their respective tasks, with distributed signal processing taking place on each node in the Node Controllers. Each node ran a Node Controller which brokers access to the USRP resource and performs on-node waveform sampling, phase–frequency correction, and ToA estimation via matched filter and QLS. Interprocess and internode communication utilized ZeroMQ over TCP/IP.

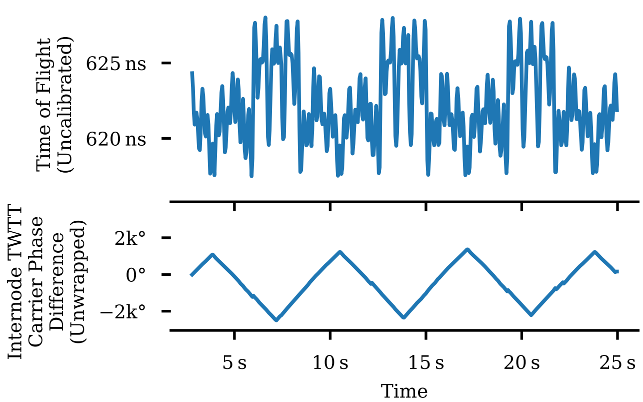

(a)

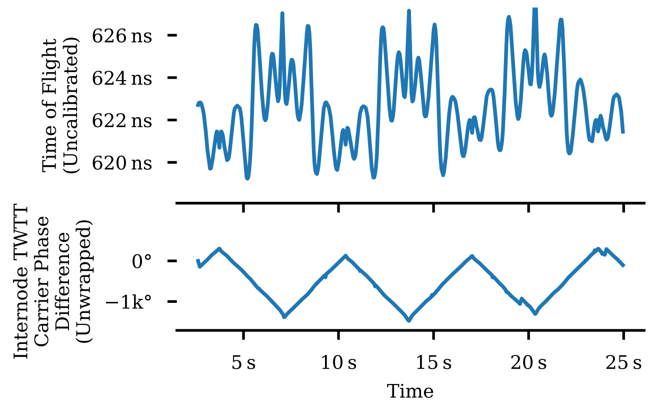

(b)

Fig. B.3. Time of flight estimates computed using (19) and unwrapped internode carrier phase differences used to indicate the approximate linear guide position for TWTT carrier frequencies of (a) 2100 MHz and (b) 700 MHz. Errors due to multipath induced by the metallic spheres at the start and end of the linear guide motion can be clearly seen in the ToF measurements.

TABLE B-II
COMPARISON OF OPEN-LOOP HIGH-ACCURACY MICROWAVE WIRELESS COORDINATION TECHNIQUES

Reference	Time Transfer Waveform	Frequency Transfer Waveform	Relative Velocity	Time Transfer SNR	Time Transfer Carrier	Bandwidth	Occupied Bandwidth	Time Standard Deviation	Frequency Standard Deviation
[38]	ultra-wideband (802.15.4a)	continuous-wave two-tone (CWTT)	0.0 m/s	NA	3.5–6.5 GHz	∼900 MHz	100 %	477 ps	NA
[78]	frequency modulated continuous-wave (FMCW)	FMCW	0.0 m/s	NA	5.725 GHz	150 MHz	100 %	66 ps	1.75 ppb
[50]	linear frequency modulation (LFM)	continuous-wave (CW) (Cabled)	0.0 m/s	NA	3.12 GHz	40 MHz	100 %	83 ps	NA
[79]	White Rabbit	CW	0.0 m/s	NA	72–75 GHz	1.6 GHz	100 %	< 2.0 ps	NA
[1]	LFM	CW (global navigation satellite system (GNSS))	0.0 m/s	31.2 dB	1.0 GHz	50 MHz	100 %	11.3 ps	NA
[43]	Pulsed CW	Pulsed CW	0.0 m/s	NA	3.07 GHz	16 kHz	100 %	NA	< 10 ppb
[46]	QAM (IEEE 1588 PTP)	QAM (IEEE 1588 PTP)	0.0 m/s	NA	NA	NA	100 %	9 ns	2 ppb
[80]	LFM	LFM	∼2.0 m/s	NA	77 GHz	1.0 GHz	100 %	330 ps	1.75 ppb
[41]	PTT	CWTT	0.0 m/s	∼36 dB	5.8 GHz	40.1 MHz	0.5 %	11 ps	NA
This Work	PTT	CWTT	0.0 m/s	∼27 dB	700 MHz	20.67 MHz	6.4 %	33 ps	NA
This Work	PTT	CWTT	0.3 m/s	∼27 dB	700 MHz	20.67 MHz	6.4 %	∼1 ns	NA
This Work	**PTT**	**PTT**	**0.0 m/s**	**∼27 dB**	**2.1 GHz**	**20.67 MHz**	**6.4 %**	**70 ps**	**∼4 ppb**
This Work	**PTT**	**PTT**	**0.3 m/s**	**∼27 dB**	**2.1 GHz**	**20.67 MHz**	**6.4 %**	**63 ps**	**∼4 ppb**

NA: Not available at time of publication

APPENDIX C
DERIVATION OF ELECTRICAL STATE RELATIONS

A. Internode Phase Difference (12)

$$\phi^{(n,m)}(t) = \phi^{(m)}(t) - \phi^{(n)}(t)$$

where $\phi^{(n)}(t) = 2\pi f_{0,\mathrm{lo}} t + \delta\phi^{(n)}(t)$, given by (4) and $\delta\phi^{(n)}(t) = 2\pi f_{0,\mathrm{lo}} \Delta f_{\mathrm{osc}}^{(n)} t + \nu_{\phi,\mathrm{lo}}^{(n)}(t) + \phi_{0,\mathrm{lo}}^{(n)}$ given by (5)

$$\begin{aligned}
&= 2\pi f_{0,\mathrm{lo}} t + \delta\phi_{\mathrm{tx}}^{(m)}(t) - 2\pi f_{0,\mathrm{lo}} t - \delta\phi_{\mathrm{tx}}^{(n)}(t) \\
&= \delta\phi_{\mathrm{tx}}^{(m)}(t) - \delta\phi_{\mathrm{tx}}^{(n)}(t) \\
&= 2\pi f_{0,\mathrm{lo}} \Delta f_{\mathrm{osc}}^{(m)} t + \nu_{\phi,\mathrm{lo}}^{(m)}(t) + \phi_{0,\mathrm{lo}}^{(m)} - \left[2\pi f_{0,\mathrm{lo}} \Delta f_{\mathrm{osc}}^{(n)} t + \nu_{\phi,\mathrm{lo}}^{(n)}(t) + \phi_{0,\mathrm{lo}}^{(n)}\right] \\
&= 2\pi f_{0,\mathrm{lo}} \left[\Delta f_{\mathrm{osc}}^{(m)} - \Delta f_{\mathrm{osc}}^{(n)}\right] t + \phi_{0,\mathrm{lo}}^{(n,m)} + \nu_{\phi,\mathrm{lo}}^{(n,m)}(t) \\
&= 2\pi f_{0,\mathrm{lo}} \Delta f_{\mathrm{osc}}^{(n,m)} t + \phi_{0,\mathrm{lo}}^{(n,m)} + \nu_{\phi,\mathrm{lo}}^{(n,m)}(t)
\end{aligned} \tag{C.1}$$

B. Apparent Time of Flight (16)

Letting $T_{\mathrm{adc}}^{(m)}(t)$ and $T_{\mathrm{dac}}^{(n)}(t)$ be PLLs defined by (2) and (3), transformed to time using (6)

$$\bar{\tau}_{\mathrm{tof}}^{(n\to m)}[k] = T_{\mathrm{adc}}^{(m)}\left(t_{\mathrm{rx}}^{(m)}[k]\right) - T_{\mathrm{dac}}^{(n)}\left(t_{\mathrm{tx}}^{(n)}[k]\right)$$

assuming $T_{0,\mathrm{adc}} = T_{0,\mathrm{dac}} = 0$ (i.e., static data converter phases are calibrated)

$$= t_{\mathrm{rx}}^{(m)}[k]\left(1 + \Delta f_{\mathrm{osc}}^{(m)}\right) + T_{0,\mathrm{sys}}^{(m)} + \frac{\nu_{\phi,\mathrm{adc}}}{2\pi f_{0,\mathrm{sys}}} - t_{\mathrm{rx}}^{(n)}[k]\left(1 + \Delta f_{\mathrm{osc}}^{(n)}\right) - T_{0,\mathrm{sys}}^{(n)} - \frac{\nu_{\phi,\mathrm{dac}}(t)}{2\pi f_{0,\mathrm{sys}}}$$

letting $t_{\mathrm{rx}}^{(m)}[k] = t_{\mathrm{tx}}^{(n)}[k] + \tau_{\mathrm{tof}}^{(n\to m)}$ and $\frac{\nu_{\phi,\mathrm{dac}}(t)}{2\pi f_{0,\mathrm{sys}}} = \nu_\phi(t)$

$$\begin{aligned}
&= \left(t_{\mathrm{tx}}^{(n)}[k] + \tau_{\mathrm{tof}}^{(n\to m)}[k]\right)\left(1 + \Delta f_{\mathrm{osc}}^{(m)}\right) - t_{\mathrm{tx}}^{(n)}\left(1 + \Delta f_{\mathrm{osc}}^{(n)}\right) + T_{0,\mathrm{sys}}^{(n,m)} + \nu_\phi(t) \\
&= \left(t_{\mathrm{tx}}^{(n)}[k] + \tau_{\mathrm{tof}}^{(n\to m)}[k]\right) + \Delta f_{\mathrm{osc}}^{(m)}\left(t_{\mathrm{tx}}^{(n)}[k] + \tau_{\mathrm{tof}}^{(n\to m)}\right) - t_{\mathrm{tx}}^{(n)}[k]\left(1 + \Delta f_{\mathrm{osc}}^{(n)}\right) + T_{0,\mathrm{sys}}^{(n,m)} + \nu_\phi(t) \\
&= t_{\mathrm{tx}}^{(n)}[k] + \tau_{\mathrm{tof}}^{(n\to m)} + \Delta f_{\mathrm{osc}}^{(m)} t_{\mathrm{tx}}^{(n)}[k] + \Delta f_{\mathrm{osc}}^{(m)} \tau_{\mathrm{tof}}^{(n\to m)} - t_{\mathrm{tx}}^{(n)}[k] - \Delta f_{\mathrm{osc}}^{(n)} t_{\mathrm{tx}}^{(n)}[k] + T_{0,\mathrm{sys}}^{(n,m)} + \nu_\phi(t) \\
&= \tau_{\mathrm{tof}}^{(n\to m)}\left(1 + \Delta f_{\mathrm{osc}}^{(m)}\right) + T_{0,\mathrm{sys}}^{(n,m)} + t_{\mathrm{tx}}^{(n)}\left(\Delta f_{\mathrm{osc}}^{(m)} - \Delta f_{\mathrm{osc}}^{(n)}\right) + \nu_\phi(t) \\
&= \tau_{\mathrm{tof}}^{(n\to m)}\left(1 + \Delta f_{\mathrm{osc}}^{(m)}\right) + T_{0,\mathrm{sys}}^{(n,m)} + \Delta f_{\mathrm{osc}}^{(n,m)} t_{\mathrm{tx}}^{(n)} + \nu_\phi(t)
\end{aligned} \tag{C.2}$$

C. Internode Time Difference Estimate (17)

Beginning with (17)

$$\begin{aligned}
\hat{T}^{(n,m)}[k] &= \frac{\bar{\tau}_{\mathrm{tof}}^{(n\to m)}[k] - \bar{\tau}_{\mathrm{tof}}^{(m\to n)}[k]}{2} \\
&= \frac{1}{2}\Big\{\Delta f_{\mathrm{osc}}^{(n,m)} t_{\mathrm{tx}}^{(n)} + \tau_{\mathrm{tof}}^{(n\to m)}\left(1 + \Delta f_{\mathrm{osc}}^{(m)}\right) + T_{0,\mathrm{sys}}^{(n,m)} + \nu_\phi(t) \\
&\qquad - \left[\Delta f_{\mathrm{osc}}^{(m,n)} t_{\mathrm{tx}}^{(m)} + \tau_{\mathrm{tof}}^{(m\to n)}\left(1 + \Delta f_{\mathrm{osc}}^{(n)}\right) + T_{0,\mathrm{sys}}^{(m,n)} + \nu_\phi(t)\right]\Big\}
\end{aligned}$$

Noting that $\Delta f_{\mathrm{osc}}^{(n,m)} = \frac{\delta f^{(m)}}{f_0} - \frac{\delta f^{(n)}}{f_0} = -\left[\frac{\delta f^{(n)}}{f_0} - \frac{\delta f^{(m)}}{f_0}\right] = -\Delta f_{\mathrm{osc}^{(\mathrm{n,m})}}$ and similarly $T_{0,\mathrm{sys}}^{(n,m)} = -T_{0,\mathrm{sys}}^{(m,n)}$, and letting the channel be quasi-static during the synchronization epoch, i.e., $\tau_{\mathrm{tof}}^{n\to m} = \tau_{\mathrm{tof}}^{m\to n} = \tau_{\mathrm{tof}}^{n\leftrightarrow m}$

$$\begin{aligned}
&= \frac{1}{2}\Big\{\Delta f_{\mathrm{osc}}^{(n,m)} t_{\mathrm{tx}}^{(n)} + \tau_{\mathrm{tof}}^{(n\leftrightarrow m)}\left(1 + \Delta f_{\mathrm{osc}}^{(m)}\right) + T_{0,\mathrm{sys}}^{(n,m)} + \nu_\phi(t) \\
&\qquad - \left[-\Delta f_{\mathrm{osc}}^{(n,m)} t_{\mathrm{tx}}^{(m)} + \tau_{\mathrm{tof}}^{(n\leftrightarrow m)}\left(1 + \Delta f_{\mathrm{osc}}^{(n)}\right) - T_{0,\mathrm{sys}}^{(n,m)} + \nu_\phi(t)\right]\Big\} \\
&= \frac{1}{2}\Big\{\Delta f_{\mathrm{osc}}^{(n,m)} t_{\mathrm{tx}}^{(n)} + \tau_{\mathrm{tof}}^{(n\leftrightarrow m)}\left(1 + \Delta f_{\mathrm{osc}}^{(m)}\right) + T_{0,\mathrm{sys}}^{(n,m)} + \nu_\phi(t) \\
&\qquad + \Delta f_{\mathrm{osc}}^{(n,m)} t_{\mathrm{tx}}^{(m)} - \tau_{\mathrm{tof}}^{(n\leftrightarrow m)}\left(1 + \Delta f_{\mathrm{osc}}^{(n)}\right) + T_{0,\mathrm{sys}}^{(n,m)} - \nu_\phi(t)\Big\}
\end{aligned}$$

$$= \frac{1}{2}\left\{\Delta f_{\rm osc}^{(n,m)}\left(t_{\rm tx}^{(n)} + t_{\rm tx}^{(m)}\right) + \tau_{\rm tof}^{(n\leftrightarrow m)}\left(\Delta f_{\rm osc}^{(m)} - \Delta f_{\rm osc}^{(n)}\right) + 2T_{0,\rm sys}^{(n,m)} + \nu_\phi(t)\right\}$$

letting $\Delta f_{\rm osc}^{(n,m)} = \Delta f_{\rm osc}^{(m)} - \Delta f_{\rm osc}^{(n)}$

$$= \frac{1}{2}\Delta f_{\rm osc}^{(n,m)}\left(t_{\rm tx}^{(n)} + t_{\rm tx}^{(m)} + \tau_{\rm tof}^{(n\leftrightarrow m)}\right) + T_{0,\rm sys}^{(n,m)} + \nu_\phi(t) \tag{C.3}$$

And simplifying if the clocks are closely synchronized $t_{\rm tx}^{(m)} \approx t_{\rm tx}^{(n)} + \tau_{\rm tdma}$ to (**??**)

$$\begin{aligned}\hat{T}^{(n,m)}[k] &\approx \frac{1}{2}\Delta f_{\rm osc}^{(n,m)}\left(2t_{\rm tx}^{(n)} + \tau_{\rm tdma} + \tau_{\rm tof}^{(n\leftrightarrow m)}\right) + T_{0,\rm sys}^{(n,m)} + \nu_\phi(t)\\ &\approx \left(\Delta f_{\rm osc}^{(n,m)} t_{\rm tx}^{(n)} + T_{0,\rm sys}^{(n,m)}\right) + \frac{1}{2}\Delta f_{\rm osc}^{(n,m)}\left(\tau_{\rm tdma} + \tau_{\rm tof}^{(n\leftrightarrow m)}\right) + \nu_\phi(t)\end{aligned}$$

the first term may then be simplified in terms of the internode time offset given by (13)

$$\approx T_{\rm sys}^{(n,m)}[k] + \frac{1}{2}\Delta f_{\rm osc}^{(n,m)}\left(\tau_{\rm tdma} + \tau_{\rm tof}^{(n\leftrightarrow m)}\right) + \nu_\phi(t) \tag{C.4}$$

D. Internode Time of Flight Estimate (19)–(20)

Starting with (19)

$$\begin{aligned}\hat{\tau}_{\rm tof}^{(n\leftrightarrow m)}[k] &= \frac{\bar{\tau}_{\rm tof}^{(n\to m)}[k] + \bar{\tau}_{\rm tof}^{(m\to n)}[k]}{2}\\ &= \frac{1}{2}\Big\{\Delta f_{\rm osc}^{(n,m)} t_{\rm tx}^{(n)} + \tau_{\rm tof}^{(n\to m)}\left(1 + \Delta f_{\rm osc}^{(m)}\right) + T_{0,\rm sys}^{(n,m)} + \nu_\phi(t)\\ &\qquad + \left[\Delta f_{\rm osc}^{(m,n)} t_{\rm tx}^{(m)} + \tau_{\rm tof}^{(m\to n)}\left(1 + \Delta f_{\rm osc}^{(n)}\right) + T_{0,\rm sys}^{(m,n)} + \nu_\phi(t)\right]\Big\}\end{aligned}$$

applying similar substitutions as in (C.3)

$$\begin{aligned}&= \frac{1}{2}\Big\{\Delta f_{\rm osc}^{(n,m)} t_{\rm tx}^{(n)} + \tau_{\rm tof}^{(n\leftrightarrow m)}\left(1 + \Delta f_{\rm osc}^{(m)}\right) + T_{0,\rm sys}^{(n,m)} + \nu_\phi(t)\\ &\qquad + \left[-\Delta f_{\rm osc}^{(n,m)} t_{\rm tx}^{(m)} + \tau_{\rm tof}^{(n\leftrightarrow m)}\left(1 + \Delta f_{\rm osc}^{(n)}\right) - T_{0,\rm sys}^{(n,m)} + \nu_\phi(t)\right]\Big\}\\ &= \frac{1}{2}\Big\{\Delta f_{\rm osc}^{(n,m)} t_{\rm tx}^{(n)} + \tau_{\rm tof}^{(n\leftrightarrow m)}\left(1 + \Delta f_{\rm osc}^{(m)}\right) + T_{0,\rm sys}^{(n,m)} + \nu_\phi(t)\\ &\qquad - \Delta f_{\rm osc}^{(n,m)} t_{\rm tx}^{(m)} + \tau_{\rm tof}^{(n\leftrightarrow m)}\left(1 + \Delta f_{\rm osc}^{(n)}\right) - T_{0,\rm sys}^{(n,m)} + \nu_\phi(t)\Big\}\\ &= \frac{1}{2}\left\{\Delta f_{\rm osc}^{(n,m)}\left(t_{\rm tx}^{(n)} - t_{\rm tx}^{(m)}\right) + \tau_{\rm tof}^{(n\leftrightarrow m)}\left(2 + \Delta f_{\rm osc}^{(n)} + \Delta f_{\rm osc}^{(m)}\right) + \nu_\phi(t)\right\}\\ &= \tau_{\rm tof}^{(n\leftrightarrow m)} + \frac{1}{2}\tau_{\rm tof}^{(n\leftrightarrow m)}\left(\Delta f_{\rm osc}^{(n)} + \Delta f_{\rm osc}^{(m)}\right) - \frac{1}{2}\Delta f_{\rm osc}^{(n,m)}\left(t_{\rm tx}^{(m)} - t_{\rm tx}^{(n)}\right) + \nu_\phi(t)\end{aligned} \tag{C.5}$$

Again simplifying if the clocks are closely synchronized $t_{\rm tx}^{(m)} \approx t_{\rm tx}^{(n)} + \tau_{\rm tdma}$

$$\hat{\tau}_{\rm tof}^{(n\leftrightarrow m)}[k] \approx \tau_{\rm tof}^{(n\leftrightarrow m)} + \frac{1}{2}\tau_{\rm tof}^{(n\leftrightarrow m)}\left(\Delta f_{\rm osc}^{(n)} + \Delta f_{\rm osc}^{(m)}\right) - \frac{1}{2}\Delta f_{\rm osc}^{(n,m)}\tau_{\rm tdma} + \nu_\phi(t) \tag{C.6}$$

And finally, once the clocks are syntonized $\Delta f_{\rm sys}^{n,m}$ becomes small, thus becoming (20)

$$\hat{\tau}_{\rm tof}^{(n\leftrightarrow m)}[k] \approx \tau_{\rm tof}^{(n\leftrightarrow m)} + \nu_\phi(t) \tag{C.7}$$

E. Fractional Frequency Estimation Error (29)

The dimensionless frequency difference between platforms can be estimated by

$$\Delta\hat{f}_{\rm osc}^{(n,m)}[k] = \frac{\hat{T}_{\rm sys}^{(n,m)}[k] - \hat{T}_{\rm sys}^{(n,m)}[k-1]}{\tau_{\rm twtt}[k]} \tag{C.8}$$

where $\tau_{\text{twtt}}[k] = t_{\text{tx}}^{(n)}[k] - t_{\text{tx}}^{(n)}[k-1]$. Expanding using (17) and (13) yields

$$\Delta\hat{f}_{\text{osc}}^{(n,m)}[k] = \frac{1}{\tau_{\text{twtt}}[k]}\Big[\Delta f_{\text{osc}}^{(n,m)}[k]t_{\text{tx}}^{(n)}[k] + T_{0,\text{sys}}^{(n,m)} + \Delta f_{\text{osc}}^{(n,m)}[k]\left(\tau_{\text{tdma}} + \tau_{\text{tof}}^{(n,m)}[k]\right)$$
$$- \Delta f_{\text{osc}}^{(n,m)}[k-1]t_{\text{tx}}^{(n)}[k-1] - T_{0,\text{sys}}^{(n,m)} - \Delta f_{\text{osc}}^{(n,m)}[k-1]\left(\tau_{\text{tdma}} + \tau_{\text{tof}}^{(n,m)}[k-1]\right)\Big]$$

Assuming that the frequency error is quasi-static over the observation interval, i.e., $\Delta f_{\text{osc}}^{(n,m)}[k] = \Delta f_{\text{osc}}^{(n,m)}[k-1]$

$$= \frac{1}{\tau_{\text{twtt}}[k]}\Delta f_{\text{osc}}^{(n,m)}[k]\left(\tau_{\text{twtt}}[k] + \tau_{\text{tof}}^{(n,m)}[k] - \tau_{\text{tof}}^{(n,m)}[k-1]\right)$$

let $\delta\tau_{\text{tof}}^{(n,m)} = \tau_{\text{tof}}^{(n,m)}[k] - \tau_{\text{tof}}^{(n,m)}[k-1]$

$$= \frac{1}{\tau_{\text{twtt}}[k]}\Delta f_{\text{osc}}^{(n,m)}[k]\left(\tau_{\text{twtt}}[k] + \delta\tau_{\text{tof}}^{(n,m)}\right)$$
$$= \Delta f_{\text{osc}}^{(n,m)}[k]\left(1 + \Delta f_{\text{osc}}^{(n,m)}[k]\frac{\delta\tau_{\text{tof}}^{(n,m)}}{\tau_{\text{twtt}}[k]}\right).$$

Assuming a line of sight (LoS) path with minimal multipath, the error term can be thought of as a radial velocity and rearranged in terms of a fraction of the radial velocity over the speed of light by

$$\frac{\delta\tau_{\text{tof}}^{(n,m)}}{\tau_{\text{twtt}}}\frac{c}{c} = \frac{\delta\tau_{\text{R}}^{(n,m)}}{\tau_{\text{twtt}}}\frac{1}{c} = \frac{v_R}{c}$$

which yields

$$\Delta\hat{f}_{\text{osc}}^{(n,m)}[k] = \Delta f_{\text{osc}}^{(n,m)}[k]\left(1 + \frac{v_R}{c}\right). \tag{C.9}$$

While $\frac{v_R}{c} << 1$, i.e., the platforms are not moving at a significant portion of the speed of light, the impact of this error will be small.

APPENDIX D
EXPERIMENTAL PARAMETERS

Description: Each figure in the follow in appendices consists of a time-domain plot of the measured quantity on the left and a probability distribution on the right. The solid trace in the time-domain plot indicates the mean value from a 500 ms time interval; the shaded region indicates the extreme values observed over that interval. Additional horizontal overlays indicate the mean μ and on standard deviation $\pm\sigma$ of 99.3 % of the data to minimize the skew due to TWTT not meeting real-time timing requirements, indicated by the solid and dashed gray lines, respectively; numeric values for these quantities are also provided as an inset in each figure.

TABLE D-I
EXP. 1: SNR EVALUATION (*Configuration A*)

Exp. #	Freq. Ref.	Frequency Offset	Velocity	Update Period	Num. Nodes	Avg. SNR	Pulse Duration	Epoch Duration	Carrier Frequency
1.1	Internal	—	0.0 m/s	44 ms	2	6	1.5 µs	10.5 µs	2100 MHz
1.2	Internal	—	0.0 m/s	44 ms	2	9	1.5 µs	10.5 µs	2100 MHz
1.3	Internal	—	0.0 m/s	44 ms	2	12	1.5 µs	10.5 µs	2100 MHz
1.4	Internal	—	0.0 m/s	44 ms	2	15	1.5 µs	10.5 µs	2100 MHz
1.5	Internal	—	0.0 m/s	44 ms	2	18	1.5 µs	10.5 µs	2100 MHz
1.6	Internal	—	0.0 m/s	44 ms	2	21	1.5 µs	10.5 µs	2100 MHz
1.7	Internal	—	0.0 m/s	44 ms	2	24	1.5 µs	10.5 µs	2100 MHz
1.8	Internal	—	0.0 m/s	44 ms	2	27	1.5 µs	10.5 µs	2100 MHz
1.9	Internal	—	0.0 m/s	44 ms	2	30	1.5 µs	10.5 µs	2100 MHz
1.10	Internal	—	0.0 m/s	44 ms	2	33	1.5 µs	10.5 µs	2100 MHz

TABLE D-II
EXP. 2: PULSE DURATION EVALUATION (*Configuration A*)

Exp. #	Freq. Ref.	Frequency Offset	Velocity	Update Period	Num. Nodes	Avg. SNR	Pulse Duration	Epoch Duration	Carrier Frequency
2.1	Internal	—	0.0 m/s	44 ms	2	30	1.5 µs	10.5 µs	2100 MHz
2.2	Internal	—	0.0 m/s	44 ms	2	30	2.0 µs	11.5 µs	2100 MHz
2.3	Internal	—	0.0 m/s	44 ms	2	30	3.0 µs	13.5 µs	2100 MHz
2.4	Internal	—	0.0 m/s	44 ms	2	30	6.0 µs	19.5 µs	2100 MHz
2.5	Internal	—	0.0 m/s	44 ms	2	30	12.0 µs	31.5 µs	2100 MHz

TABLE D-III
EXP. 3: SYNCHRONIZATION EPOCH DURATION EVALUATION (*Configuration A*)

Exp. #	Freq. Ref.	Frequency Offset	Velocity	Update Period	Num. Nodes	Avg. SNR	Pulse Duration	Epoch Duration	Carrier Frequency
3.1	Internal	—	0.0 m/s	44 ms	2	30	1.5 µs	10.5 µs	2100 MHz
3.2	Internal	—	0.0 m/s	44 ms	2	30	1.5 µs	13.5 µs	2100 MHz
3.3	Internal	—	0.0 m/s	44 ms	2	30	1.5 µs	19.5 µs	2100 MHz
3.4	Internal	—	0.0 m/s	44 ms	2	30	1.5 µs	31.5 µs	2100 MHz
3.5	Internal	—	0.3 m/s	44 ms	2	30	1.5 µs	10.5 µs	2100 MHz
3.6	Internal	—	0.3 m/s	44 ms	2	30	1.5 µs	13.5 µs	2100 MHz
3.7	Internal	—	0.3 m/s	44 ms	2	30	1.5 µs	19.5 µs	2100 MHz
3.8	Internal	—	0.3 m/s	44 ms	2	30	1.5 µs	31.5 µs	2100 MHz

TABLE D-IV
EXP. 4: RESYNCHRONIZATION PERIOD EVALUATION (*Configuration A*)

Exp. #	Freq. Ref.	Frequency Offset	Velocity	Update Period	Num. Nodes	Avg. SNR	Pulse Duration	Epoch Duration	Carrier Frequency
4.1	Internal	—	0.0 m/s	44 ms	2	30	1.5 µs	10.5 µs	2100 MHz
4.2	Internal	—	0.0 m/s	45 ms	2	30	1.5 µs	10.5 µs	2100 MHz
4.3	Internal	—	0.0 m/s	46 ms	2	30	1.5 µs	10.5 µs	2100 MHz
4.4	Internal	—	0.0 m/s	47 ms	2	30	1.5 µs	10.5 µs	2100 MHz
4.5	Internal	—	0.0 m/s	48 ms	2	30	1.5 µs	10.5 µs	2100 MHz
4.6	Internal	—	0.0 m/s	50 ms	2	30	1.5 µs	10.5 µs	2100 MHz

TABLE D-V
EXP. 5: NODE SCALING EVALUATION (*Configuration A*)

Exp. #	Freq. Ref.	Frequency Offset	Velocity	Update Period	Num. Nodes	Avg. SNR	Pulse Duration	Epoch Duration	Carrier Frequency
5.1	Internal	—	0.0 m/s	44 ms	2	30	1.5 µs	10.5 µs	2100 MHz
5.2	Internal	—	0.0 m/s	50 ms	3	30	1.5 µs	10.5 µs	2100 MHz
5.3	Internal	—	0.0 m/s	55 ms	4	30	1.5 µs	10.5 µs	2100 MHz
5.4	Internal	—	0.3 m/s	44 ms	2	30	1.5 µs	10.5 µs	2100 MHz
5.5	Internal	—	0.3 m/s	50 ms	3	30	1.5 µs	10.5 µs	2100 MHz
5.6	Internal	—	0.3 m/s	55 ms	4	30	1.5 µs	10.5 µs	2100 MHz

TABLE D-VI
EXP. 6: FREQUENCY OFFSET EVALUATION (*Configuration B*)

Exp. #	Freq. Ref.	Frequency Offset	Velocity	Update Period	Num. Nodes	Avg. SNR	Pulse Duration	Epoch Duration	Carrier Frequency
6.1	Cabled	0.0 Hz	0.0 m/s	44 ms	2	30	1.5 µs	10.5 µs	2100 MHz
6.2	Cabled	0.01 Hz	0.0 m/s	44 ms	2	30	1.5 µs	10.5 µs	2100 MHz
6.3	Cabled	0.1 Hz	0.0 m/s	44 ms	2	30	1.5 µs	10.5 µs	2100 MHz
6.4	Cabled	1.0 Hz	0.0 m/s	44 ms	2	30	1.5 µs	10.5 µs	2100 MHz
6.5	Cabled	10 Hz	0.0 m/s	44 ms	2	30	1.5 µs	10.5 µs	2100 MHz
6.6	Cabled	100Hz	0.0 m/s	44 ms	2	30	1.5 µs	10.5 µs	2100 MHz
6.7	Internal	—	0.0 m/s	44 ms	2	30	1.5 µs	10.5 µs	2100 MHz
6.8	Cabled	0.0 Hz	0.3 m/s	44 ms	2	30	1.5 µs	10.5 µs	2100 MHz
6.9	Cabled	0.01 Hz	0.3 m/s	44 ms	2	30	1.5 µs	10.5 µs	2100 MHz
6.10	Cabled	0.1 Hz	0.3 m/s	44 ms	2	30	1.5 µs	10.5 µs	2100 MHz
6.11	Cabled	1.0 Hz	0.3 m/s	44 ms	2	30	1.5 µs	10.5 µs	2100 MHz
6.12	Cabled	10 Hz	0.3 m/s	44 ms	2	30	1.5 µs	10.5 µs	2100 MHz
6.13	Cabled	100Hz	0.3 m/s	44 ms	2	30	1.5 µs	10.5 µs	2100 MHz
6.14	Internal	—	0.3 m/s	44 ms	2	30	1.5 µs	10.5 µs	2100 MHz

TABLE D-VII
EXP. 8: ANALOG CWTT AND DIGITAL TIME-FREQUENCY COORDINATION EVALUATION (*Configuration C*)

Exp. #	Freq. Ref.	Frequency Offset	Velocity	Update Period	Num. Nodes	Avg. SNR	Pulse Duration	Epoch Duration	Carrier Frequency
8.1	WFT*	—	0.003 m/s	44 ms	2	30	1.5 µs	10.5 µs	700 MHz
8.2	WFT*	—	0.03 m/s	44 ms	2	30	1.5 µs	10.5 µs	700 MHz
8.3	WFT*	—	0.3 m/s	44 ms	2	30	1.5 µs	10.5 µs	700 MHz
8.4	WFT*	—	0.0 m/s	44 ms	2	30	1.5 µs	10.5 µs	700 MHz
8.5	Internal	—	0.0 m/s	44 ms	2	30	1.5 µs	10.5 µs	700 MHz
8.6	Internal	—	0.3 m/s	44 ms	2	30	1.5 µs	10.5 µs	700 MHz
8.7	Internal	—	0.03 m/s	44 ms	2	30	1.5 µs	10.5 µs	700 MHz
8.8	Internal	—	0.003 m/s	44 ms	2	30	1.5 µs	10.5 µs	700 MHz

* External analog continuous-wave two-tone (CWTT) wireless frequency transfer circuit

TABLE D-VIII
EXP. 21: SNR EVALUATION OF BEAMFORMING FREQUENCY STABILITY (*Configuration A*)

Exp. #	Freq. Ref.	Frequency Offset	Velocity	Update Period	Num. Nodes	Avg. SNR	Pulse Duration	Epoch Duration	Carrier Frequency	BF Pulse Duration
21.1	Internal	—	0.0 m/s	44 ms	2	6	1.5 µs	10.5 µs	2100 MHz	100 µs
21.2	Internal	—	0.0 m/s	44 ms	2	9	1.5 µs	10.5 µs	2100 MHz	100 µs
21.3	Internal	—	0.0 m/s	44 ms	2	12	1.5 µs	10.5 µs	2100 MHz	100 µs
21.4	Internal	—	0.0 m/s	44 ms	2	15	1.5 µs	10.5 µs	2100 MHz	100 µs
21.5	Internal	—	0.0 m/s	44 ms	2	18	1.5 µs	10.5 µs	2100 MHz	100 µs
21.6	Internal	—	0.0 m/s	44 ms	2	21	1.5 µs	10.5 µs	2100 MHz	100 µs
21.7	Internal	—	0.0 m/s	44 ms	2	24	1.5 µs	10.5 µs	2100 MHz	100 µs
21.8	Internal	—	0.0 m/s	44 ms	2	27	1.5 µs	10.5 µs	2100 MHz	100 µs
21.9	Internal	—	0.0 m/s	44 ms	2	30	1.5 µs	10.5 µs	2100 MHz	100 µs
21.10	Internal	—	0.0 m/s	44 ms	2	33	1.5 µs	10.5 µs	2100 MHz	100 µs

TABLE D-IX
EXP. 26: FREQUENCY OFFSET EVALUATION OF BEAMFORMING FREQUENCY STABILITY (*Configuration B*)

Exp. #	Freq. Ref.	Frequency Offset	Velocity	Update Period	Num. Nodes	Avg. SNR	Pulse Duration	Epoch Duration	Carrier Frequency	BF Pulse Duration
26.1	Cabled	0.0 Hz	0.0 m/s	44 ms	2	30	1.5 µs	10.5 µs	2100 MHz	100 µs
26.2	Cabled	0.01 Hz	0.0 m/s	44 ms	2	30	1.5 µs	10.5 µs	2100 MHz	100 µs
26.3	Cabled	0.1 Hz	0.0 m/s	44 ms	2	30	1.5 µs	10.5 µs	2100 MHz	100 µs
26.4	Cabled	1.0 Hz	0.0 m/s	44 ms	2	30	1.5 µs	10.5 µs	2100 MHz	100 µs
26.5	Cabled	10 Hz	0.0 m/s	44 ms	2	30	1.5 µs	10.5 µs	2100 MHz	100 µs
26.6	Cabled	100 Hz	0.0 m/s	44 ms	2	30	1.5 µs	10.5 µs	2100 MHz	100 µs
(21.10)	Internal	—	0.0 m/s	44 ms	2	30	1.5 µs	10.5 µs	2100 MHz	100 µs
26.8	Cabled	0.0 Hz	0.3 m/s	44 ms	2	30	1.5 µs	10.5 µs	2100 MHz	100 µs
26.9	Cabled	0.01 Hz	0.3 m/s	44 ms	2	30	1.5 µs	10.5 µs	2100 MHz	100 µs
26.10	Cabled	0.1 Hz	0.3 m/s	44 ms	2	30	1.5 µs	10.5 µs	2100 MHz	100 µs
26.11	Cabled	1.0 Hz	0.3 m/s	44 ms	2	30	1.5 µs	10.5 µs	2100 MHz	100 µs
26.12	Cabled	10 Hz	0.3 m/s	44 ms	2	30	1.5 µs	10.5 µs	2100 MHz	100 µs
26.13	Cabled	100 Hz	0.3 m/s	44 ms	2	30	1.5 µs	10.5 µs	2100 MHz	100 µs
26.14	Internal	—	0.3 m/s	44 ms	2	30	1.5 µs	10.5 µs	2100 MHz	100 µs